Materials Today Chemistry 30 (2023) 101525

Contents lists available at ScienceDirect

Materials Today Chemistry

journal homepage: www.journals.elsevier.com/materials-today-chemistry/

Biobased supramolecular ionic networks with optimized crystallinity and mechanical properties as promising dynamic materials for eutectogels design

L.I. Ronco [a, b, **], G.C. Luque [a, b], C.A. Calderón [c], E.M. Euti [c], E. Rufeil Fiori [c], D.E. Barraco [c], E.P.M. Leiva [d], D. Mecerreyes [e, f], R.J. Minari [a, b], M.L. Picchio [a, e, *]

[a] Instituto de Desarrollo Tecnológico para la Industria Química (INTEC), CONICET, Güemes 3450, Santa Fe 3000, Argentina
[b] Faculta de Ingeniería Química, Universidad Nacional Del Litoral, Santiago Del Estero 2829, Santa Fe 3000, Argentina
[c] Facultad de Matemática, Astronomía, Física y Computación, Universidad Nacional de Córdoba, Instituto de Física Enrique Gaviola, Av. Medina Allende S/n, Ciudad Universitaria, Córdoba 5000, Argentina
[d] Facultad de Ciencias Químicas (Universidad Nacional de Córdoba), Haya de la Torre Esq. Medina Allende, Ciudad Universitaria, Instituto de Investigaciones en Fisicoquímica de Córdoba, Córdoba 5000, Argentina
[e] POLYMAT, Applied Chemistry Department, Faculty of Chemistry, University of the Basque Country UPV/EHU, Paseo Manuel de Lardizabal 3, Donostia-San Sebastián 20018, Spain
[f] IKERBASQUE, Basque Foundation for Science, Plaza Euskadi 5, 48009, Bilbao, Spain

ARTICLE INFO

Article history:
Received 22 November 2022
Received in revised form
16 February 2023
Accepted 23 March 2023
Available online 17 April 2023

Keywords:
Semicrystalline networks
Fatty diamines
Natural acids
Deep eutectic solvents
Sustainable eutectogels

ABSTRACT

Ionic supramolecular networks are attractive materials for technological applications with unique properties such as ionic conductivity, stimuli-responsiveness, recyclability, and self-healing. Herein, new semicrystalline supramolecular ionic networks are designed from fully biobased building blocks such as tartaric acid, phytic acid, sebacic acid, and a fatty dimer diamine (Priamine™ 1071). The combination of tartaric acid with Priamine™ 1071 results in a crystalline and brittle polymer, but its molecular regularity can be controlled by incorporating sebacic acid or phytic acid, affording tough materials with appropriate mechanical properties (elastic moduli ranging 19–42 MPa). Furthermore, the ionic polymers show network-to-liquid phase transitions between 75 and 127 °C, and in the liquid state, they were found to be miscible with a lithium-based deep eutectic solvent, yielding flexible and conductive eutectogels. Altogether, these dynamic networks could open new prospects for developing fully green soft ionic materials from their combination with other innovative and low-cost eutectic mixtures.

1. Introduction

Supramolecular ionic interactions represent a real opportunity to design new intelligent and functional polymer materials holding great promise in the field of actuators [1], sensors [2], and advanced energy-storage devices [3]. A simple proton transfer reaction between multifunctional carboxylic acids and amines can be used to introduce these ionic interactions in polymer networks readily [4]. Due to their dynamic nature, the resulting materials often show stimuli-response, shape-memory, recyclability, or self-healing properties that are invaluable for high-demanding applications [5–7]. Since the discovery of supramolecular ionic networks by Prof. Grinstaff in 2008 [8], this realm has been considerably expanded, incorporating a variety of ionic motifs and polymer architectures [9–12]. For instance, Mecerreyes et al. pioneered the development of ionic networks combining aliphatic diamines/natural dicarboxylic acids [13,14], geminal dicationic ionic liquids/citric acid [15], sulfonyl imide dianions/geminal di-imidazolium dications [16], and fully biobased building blocks [17]. This last class of networks is especially fascinating, considering a sustainable and versatile design made 100% from biobased materials.

Interestingly, biobased ionic supramolecular networks derived from fatty dimer diamine (Priamine™ 1074) and tartaric acid (TA) have been reported as semicrystalline [17]. Crystalline domains in polymer networks are, in most cases, beneficial as they contribute

* Corresponding author.
** Corresponding author.
E-mail addresses: lronco@santafe-conicet.gov.ar (L.I. Ronco), matiasluis.picchiop@ehu.eus (M.L. Picchio).

https://doi.org/10.1016/j.mtchem.2023.101525

to improving their mechanical and thermal stability [18,19]. Unfortunately, as in the case of Priamine™ 1074/TA, great crystallinity extents turn the materials highly brittle. In addition, it has been demonstrated that high crystallinity can negatively affect ionic conductivity in polymer electrolytes [20–23].

Therefore, in this communication, we propose that by controlling the molecular regularity in tartaric-based ionic networks, their crystallization degree could be tuned-up, giving rise to new ionic polymers with boosted mechanical performance. In this vein, we used natural long-chain dicarboxylic and multifunctional acids to break the hydrogen bond-induced crystallization in those ionic networks. Specifically, ionic polymers were prepared by proton transfer reaction combining all plant-derived Priamine™ 1071, TA, sebacic acid (SA), and phytic acid (PA), a multifunctional ionic crosslinker frequently used in conductive materials [24,25]. The obtained ionic networks were characterized in terms of their viscoelastic, thermal, mechanical, and ionic properties. Furthermore, since these dynamic polymers show thermoreversible network-to-liquid phase transitions, they could be appealing platforms to immobilize neoteric ionic solvents like deep eutectic solvents (DES), toward developing innovative eutectogels. As proof of this, we explore the use of lithium bis [(trifluoromethyl)sulfonyl] imide (LiTFSI) and N-methylacetamide (NMA) (1: 2 mol ratio) to yield flexible eutectogels as potential polymer electrolyte for lithium metal batteries. Indeed, LiTFSI/NMA has already proved to be an efficient and low-cost electrolyte for lithium-activated carbon-based supercapacitors [26–28], Li-ion, and lithium metal batteries [29–31]. Thus, it is expected that ionic network-based eutectogels bring new perspectives to the design of energy-storage devices.

2. Results and discussion

2.1. Synthesis and characterization of supramolecular ionic networks

Herein, we explored the synthesis of supramolecular ionic networks by a proton transfer reaction between Brønsted acids (i.e., dicarboxylic acids) and a Brønsted base (i.e., diamine), as presented in Fig. 1A [14,32]. Commercially available reagents entirely based on 100% renewable carbon were used, including two dicarboxylic acids, such as TA and SA, multifunctional PA, and the diamine Priamine™ 1071. All synthesized ionic networks were prepared using equal equivalents of diamine and diacids, varying the chemical nature of the acid feed composition. The equivalent fractions of each acid are indicated in the experiment codes as a subscript after

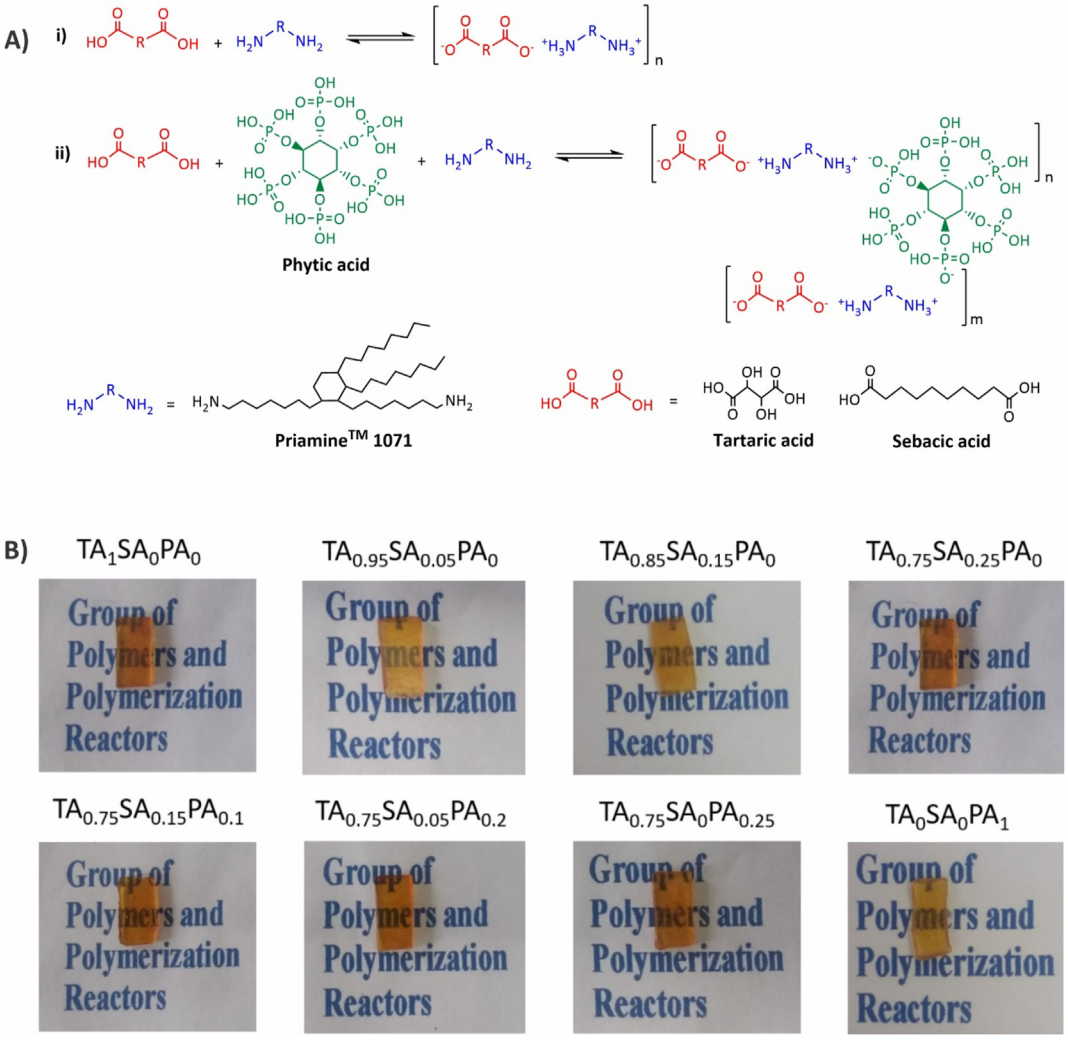

Fig. 1. Proposed reaction route for the synthesis of the supramolecular ionic networks. Priamine™ 1071 is represented with an ideal structure (A). Pictures of the as-prepared ionic networks (B).

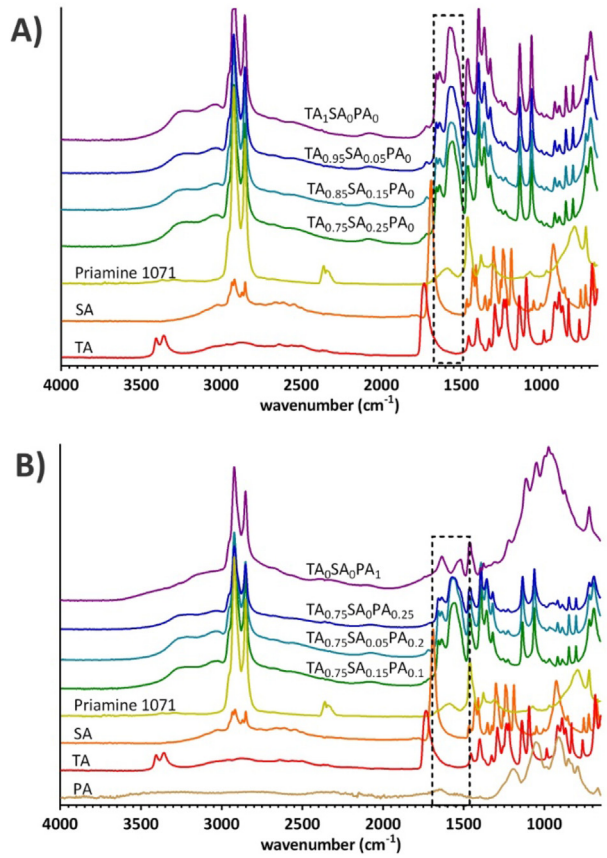

Fig. 2. ATR-FTIR spectrums of the synthesized supramolecular ionic networks based on tartaric acid, sebacic acid, and Priamine™ 1071, without (A) and with phytic acid (B).

Table 1
Thermal properties of the synthesized ionic networks measured by differential scanning calorimetry and crystallinity degrees estimated by X-ray diffraction.

Ionic network	T_g (°C)[a]	T_m (°C)[b]	A_m (J/g)	Crystallinity (%)
$TA_1SA_0PA_0$	N.D.	140.1	33.0	42.0
$TA_{0.95}SA_{0.05}PA_0$	N.D	137.2	30.6	33.9
$TA_{0.85}SA_{0.15}PA_0$	N.D	140.3	27.5	28.3
$TA_{0.75}SA_{0.25}PA_0$	−26.8	121.4	15.5	20.7
$TA_{0.75}SA_{0.15}PA_{0.1}$	−31.0	106.3	12.3	29.3
$TA_{0.75}SA_{0.05}PA_{0.2}$	−24.4	109.2	15.5	23.1
$TA_{0.75}SA_0PA_{0.25}$	−15.1	114.4	23.0	35.8
$TA_0SA_0PA_1$	−12.8	72.8	16.2	23.4

[a] Determined from the second heating cycle.
[b] Determined from the first heating cycle; N.D.: Not detected.

the abbreviations “TA” for tartaric acid, “SA” for sebacic acid, and “PA” for phytic acid. Thus, $TA_{0.75}SA_{0.25}PA_0$ indicates an ionic network synthesized with an equivalent ratio of TA/SA/PA equal to 0.75/0.25/0.

Note that the incorporation of PA gives place to the formation of multiple ionic interactions, acting like a physical crosslinker of the 3D network. In addition, the presence of TA, containing hydroxyl functionalities, can induce crystallization in the network by hydrogen bonding interactions. The formed ionic materials (Fig. 1B) presented a brownish color and were transparent.

Fig. 2 shows the attenuated total reflectance Fourier transform infrared (ATR-FTIR) spectra of the ionic networks and their pure components. For Priamine™ 1071, peaks at 2920 and 2850 cm^{-1} are attributed to CH_2 symmetrical and asymmetrical stretching. The C=O stretching band of TA and SA appears at 1730 and 1690 cm^{-1}, respectively, while peaks at 3405, 3360 cm^{-1} and 1150, 1100 cm^{-1} in the spectrum of TA are associated with −OH and C−O stretching vibrations, respectively. In the spectrum of all synthesized ionic networks, a new intense peak can be observed at 1560 cm^{-1}, which corresponds to the (COO) asymmetrical stretching of carboxylate anions, evidencing the proton transfer reaction between the acids and the amine to form the ionic species. Moreover, a significant red-shift of the −OH and C−O stretching bands of TA was observed after forming the ionic materials, indicating strong hydrogen bonding interactions.

The crystallinity degree of the networks induced by these hydrogen bonding interactions was investigated by thermal analysis. Fig. 3A and B, and Fig. S1 of the supporting information (SI) show the differential scanning calorimetry (DSC) curves of the first and second heating cycle, respectively, while Table 1 presents the values of T_g, T_m, and the area of the melting peak (A_m) that is related to the extent of crystallinity in the ionic networks.

As can be observed for ionic networks synthesized without PA, T_m, and A_m decreased when the concentration of TA was diminished, indicating a reduction in the formation of semicrystalline regions (Table 1, Fig. 3A). Furthermore, a T_g at low temperature is observed in the material with a TA concentration of 0.75 Eqv. ($TA_{0.75}SA_{0.25}PA_0$), while it is not detected in ionic networks with higher content of this acid. This behavior can be associated with the increment in crystallinity extent, as crystalline domains act as physical crosslinks and reduce the polymer chain mobility.

On the other hand, the effect of PA can be evaluated according to its concentration. For instance, when a low amount of this acid is used, as in $TA_{0.75}SA_{0.15}PA_{0.1}$, T_g, T_m, and A_m were reduced compared to the analogous ionic network $TA_{0.75}SA_{0.25}PA_0$. These effects can probably be related to the large molecular size of PA, which can increase the free volume of the network reducing the T_g. Although PA can act as a physical multifunctional crosslinker, restricting the polymer chain mobility and hence increasing the T_g, it is supposed that, at low concentrations, the increment of the network's free volume dominates the effect on the phase transition. In addition, low PA contents can introduce more network irregularities by reducing the crystallinity and, therefore, T_m and A_m.

However, higher PA concentrations ($TA_{0.75}SA_{0.05}PA_{0.2}$ and $TA_{0.75}SA_0PA_{0.25}$) increased the T_g, T_m, and A_m. This effect on the T_g could be a consequence of both the multiple functionalities of PA and the increment in the crystallinity, which augment the restriction in the polymer chain mobility. On the other hand, to understand the increment on A_m, it should be considered that the ionic network synthesized using only PA ($TA_0SA_0PA_1$) also presented crystallinity but with a T_m at a lower temperature (72.8 °C) compared to materials with TA. Note that for samples $TA_{0.75}SA_{0.15}PA_{0.1}$, $TA_{0.75}SA_{0.05}PA_{0.2}$, and $TA_{0.75}SA_0PA_{0.25}$, the onset of the melting peak happened at lower temperatures, similar to that of the ionic network $TA_0SA_0PA_1$ (Fig. 3B), resulting in broader phase transitions.

X-ray diffraction (XRD) patterns confirm the semicrystalline structure of these ionic networks, which present a high proportion of amorphous content, denoted by a broad peak around 20°. In addition, crystalline reflections are observed, some of which have a

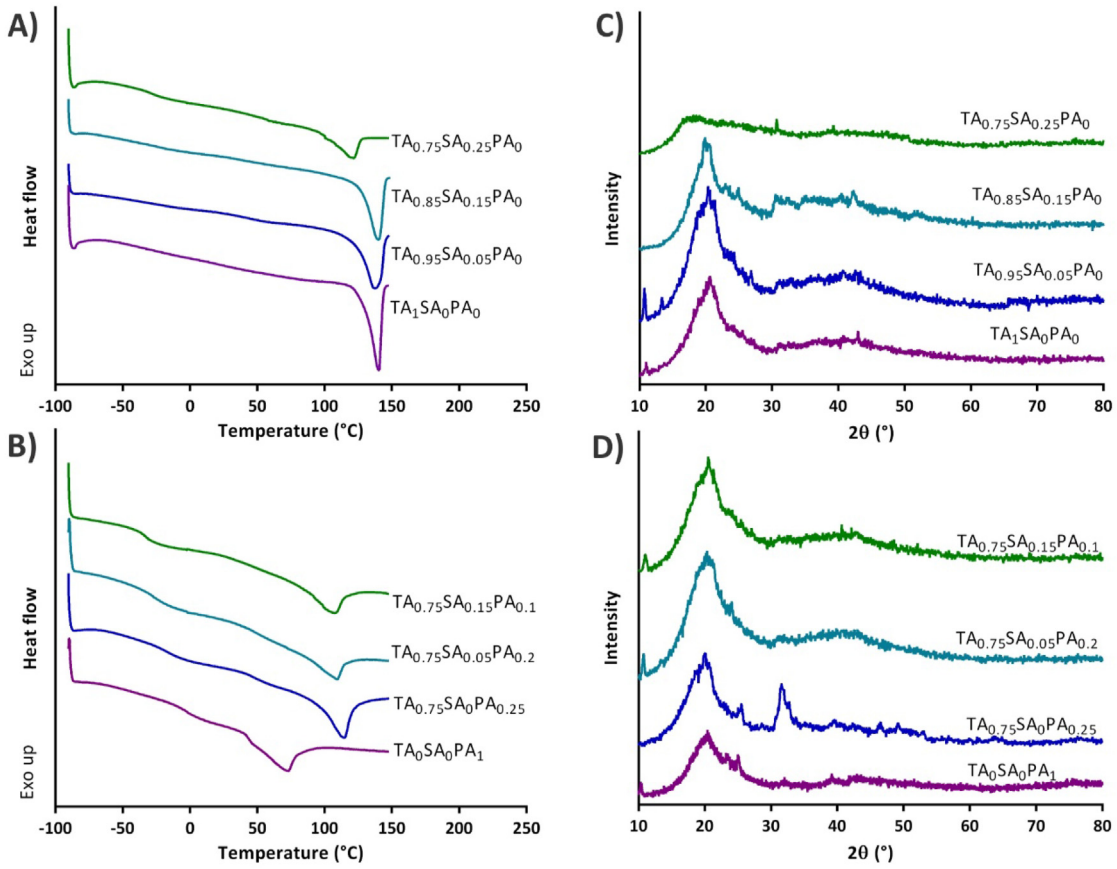

Fig. 3. Differential scanning calorimetry curves corresponding to the first heating cycle and X-ray diffraction patterns of ionic networks based on tartaric acid, sebacic acid, and Priamine™ 1071, without (A,C) and with phytic acid (B,D).

narrow full-width half maximum, denoting the presence of small-sized crystals (Fig. 3C and D). A similar XRD pattern can be observed for most ionic networks, except for the sample synthesized from TA and PA ($TA_{0.75}SA_0PA_{0.25}$), which exhibited an important crystalline reflection at 31.5°, which does not appear in the ionic networks with only TA ($TA_1SA_0PA_0$) or PA ($TA_0SA_0PA_1$). There is no clear explanation for this result, but we surmise that a new crystalline structure could be formed due to hydrogen bonding interactions between TA and PA. Evidence of these interactions was obtained by the ATR-FTIR analysis of a mixture of TA and PA, which shows shifts to lower wavenumber in the C=O (1730 cm^{-1}) and C–O (1150 and 1100 cm^{-1}) stretching bands of TA, associated with hydrogen bonding (Fig. S2 of the SI).

Crystallinity was estimated using the ratio between the area of the main crystalline reflections and the total area of the peaks (crystalline and amorphous), where the amorphous contributions were chosen as the broader peaks. In order to deconvolve the crystalline and amorphous areas, the commercial software PeakFit™ was used. An example of the fitting procedure is shown in Fig. S3 of the SI. According to this analysis, ionic networks present crystallinity degrees between 20 and 42% (Table 1), depending on their composition. These crystallinity degree values are consistent with the A_m values obtained by DCS.

Altogether, these results unveil that the crystallinity of the supramolecular ionic materials can be modulated by breaking the molecular regularity of the networks induced by the TA-promoted hydrogen bonding interactions.

Next, the thermal stability of the supramolecular ionic networks was analyzed by thermogravimetric analysis. All the synthesized materials were thermally stable until 170 °C in air, showing similar degradation profiles (Fig. 4), with temperatures at the maximal decomposition rate ($T_{d,max}$) ranging from 432 to 446 °C. The onset of the degradation process of the ionic networks agrees with the decomposition of SA and TA (Fig. S4 of the SI).

Moreover, the viscoelastic behavior of these ionic materials was investigated by dynamic mechanical thermal analysis. The rheological functions storage modulus (G′), loss modulus (G″), and tan δ versus temperature are presented in Fig. 5 and Fig. S5 of the SI. For $TA_1SA_0PA_0$ and $TA_{0.95}SA_{0.05}PA_0$ networks, a T_g (as a maximum in tan δ) can be observed at 56 and 46 °C, respectively, which was not detected by DSC. Considering the T_g of $TA_{0.75}SA_{0.25}PA_0$ (−26.8 °C) determined by DSC, this phase transition follows an increasing trend with the TA content, probably due to the promotion of hydrogen bonding interactions. This result agrees with the increase in the crystallinity at higher TA contents.

Curiously, $TA_{0.95}SA_{0.05}PA_0$ showed an increase in G′ and G″ between 30 and 40 °C, close to the T_g detected as a peak in tan δ (46 °C), probably due to cold crystallization. We surmise that this ionic network could have a wide T_g that is overlapped with the cold crystallization process. To corroborate this hypothesis, a

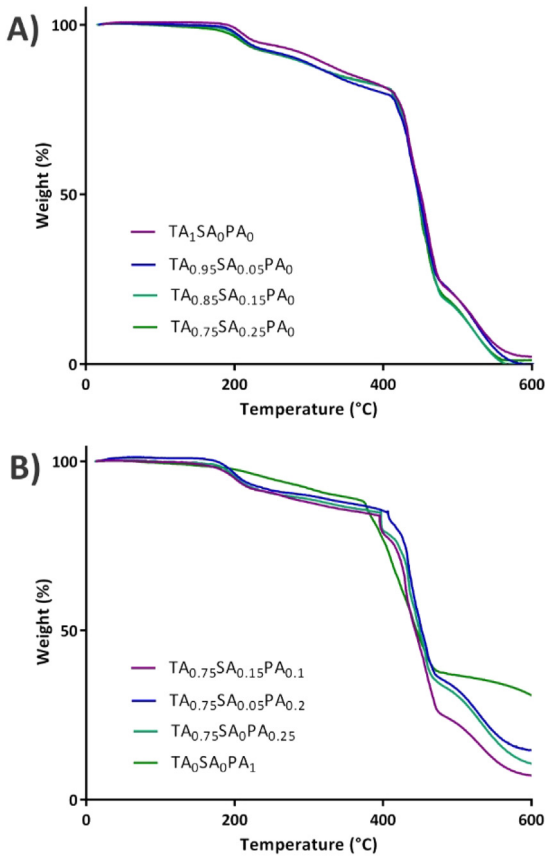

Fig. 4. Thermogravimetric analysis curves of supramolecular ionic networks based on tartaric acid, sebacic acid, and Priamine™ 1071.

modulated DSC was performed (Fig. S6 of SI). Unfortunately, a T_g could not be detected in the reversing signal, possibly due to the high crystalline degree of this sample. However, the non-reversing signal shows a small exothermal peak in the temperature range of 0–40 °C, which is consistent with a cold crystallization process.

A viscoelastic behavior with G' > G″ is observed at low temperatures and above the T_g for each sample, but due to the supramolecular nature of the ionic networks, all of them exhibited a solid-liquid transition at higher temperatures. The transition temperature from viscoelastic network to viscoelastic liquid (T_{nl}) was defined as the temperatures at which G' = G'' (Fig. 5 and Fig. S5). Note that T_{nl} is associated with the extent of the network's crystallinity since, in highly crystalline materials, T_{nl} happens at higher temperatures. In addition, in materials with high crystallinity, the transition is determined by the crystals melting, which is observed by a fast decrease of both moduli in the range of 120–140 °C, consistent with the T_m determined by DSC.

However, in the ionic networks with low crystallinity, such as $TA_{0.85}SA_{0.15}PA_0$, $TA_{0.75}SA_{0.25}PA_0$, and $TA_{0.75}SA_{0.15}PA_{0.1}$, the solid-liquid transition occurs at temperatures significantly lower than the melting process.

Uniaxial compression tests were performed to characterize the mechanical properties of the supramolecular ionic networks. Fig. 6A and B present the compression stress-strain curves, and the corresponding global values are summarized in Fig. 6C and D and Table S2. The synthesized ionic networks showed a region of linear elastic deformation followed by a plastic deformation region. Softer materials were obtained at lower content of TA, showing a decreasing tendency in the compressive modulus, yield strength, and compressive strength at 35% of strain. For instance, the compressive modulus decayed from ≈42 to 19 MPa and the yield strength from ≈11 to 4 MPa for $TA_1SA_0PA_0$ and $TA_{0.75}SA_{0.25}PA_0$, respectively. This behavior is attributed to the reduced extent of the network's crystallinity at lower TA contents. In addition, the higher amorphous fraction in samples with increased SA amount reduced the elastic deformation region (i.e., lower yield strain). The effect of the incorporation of PA can be appreciated as an increment in the yield strength, yield strain, and compressive strength at 35% of strain (Fig. 6C and D and Table S2), as a consequence of both PA acting as a physical multifunctional crosslinker and the increase of the network's crystallinity.

All in all, by modulating the chemical nature and feeding ratio of the natural acids, the crystallinity extent of the ionic networks can be controlled, affording materials with proper mechanical performance.

2.2. Supramolecular ionic networks for eutectogels design

Given the ionic and dynamic nature of the obtained supramolecular networks, they could be appealing materials to support ionic solvents, such as the emerging family of DES. As an example, we explored the embedment of LiTFSI/NMA (1: 2) DES and evaluated the performance of the resulting eutectogels as gel electrolytes for lithium metal batteries. $TA_{0.75}SA_{0.25}PA_0$ and $TA_{0.75}SA_{0.15}PA_{0.1}$ materials were selected because they contain a higher amorphous content, as high crystallinity could negatively affect ionic conductivity in solid polymer electrolytes.

Both ionic networks were doped with 10% of LiTFSI/NMA (1: 2) DES (Fig. S7). The DSC results show a similar extent of crystallinity compared to materials without DES and a slight increase in the T_g (Table S3). These results do not fit with what is expected for low molecular weight liquids plasticizing traditional polymer materials, reducing their T_g and crystallinity degree. However, the ionic nature of the network and DES could promote their interaction, restricting the mobility of the polymer chains.

In addition, the T_{nl} determined by rheology was reduced to 65 and 62 °C for $TA_{0.75}SA_{0.25}PA_0$ and $TA_{0.75}SA_{0.15}PA_{0.1}$, respectively, when 10 wt% of DES was incorporated (Fig. 7A and B). Interestingly, softer ionic networks were obtained with lower compressive modulus and strength (Fig. 7C and Table S2). Moreover, the DES-doped ionic network presents good flexibility (Video S1 of the SI) and can be bent while maintaining the deformed shape. Besides, it is possible to return the ionic network to its original shape without changes in its appearance (Fig. 7D).

Supplementary video related to this article can be found at https://doi.org/10.1016/j.mtchem.2023.101525

The ionic conductivity of the membranes at room temperature was determined by electrochemical impedance spectroscopy measurements, and the results are summarized in Table S4. For $TA_{0.75}SA_{0.15}PA_{0.1}$ and $TA_{0.75}SA_{0.25}PA_0$, the ionic conductivity considerably increases up to $\approx 10^{-4}$ S/cm when DES is incorporated due to the increase of ion carrier concentration from the lithium salt addition. It is worth mentioning that these conductivity values are in the same order of magnitude as the typically used commercial Celgard 2325 (Table S4).

Then, symmetric Li-membrane-Li cells were assembled and cycled at several current densities. The cell assembled with $TA_{0.75}SA_{0.15}PA_{0.1}$ shows no activity when a current is applied (Li^+ from the added electrolyte does not pass through the membrane). Interestingly, the cell assembled with $TA_{0.75}SA_{0.15}PA_{0.1}$-DES (10%), which exhibits an improved ionic conductivity, can be cycled at 5 μA/cm^2 (Fig. S8). Nevertheless, the potential profile is not

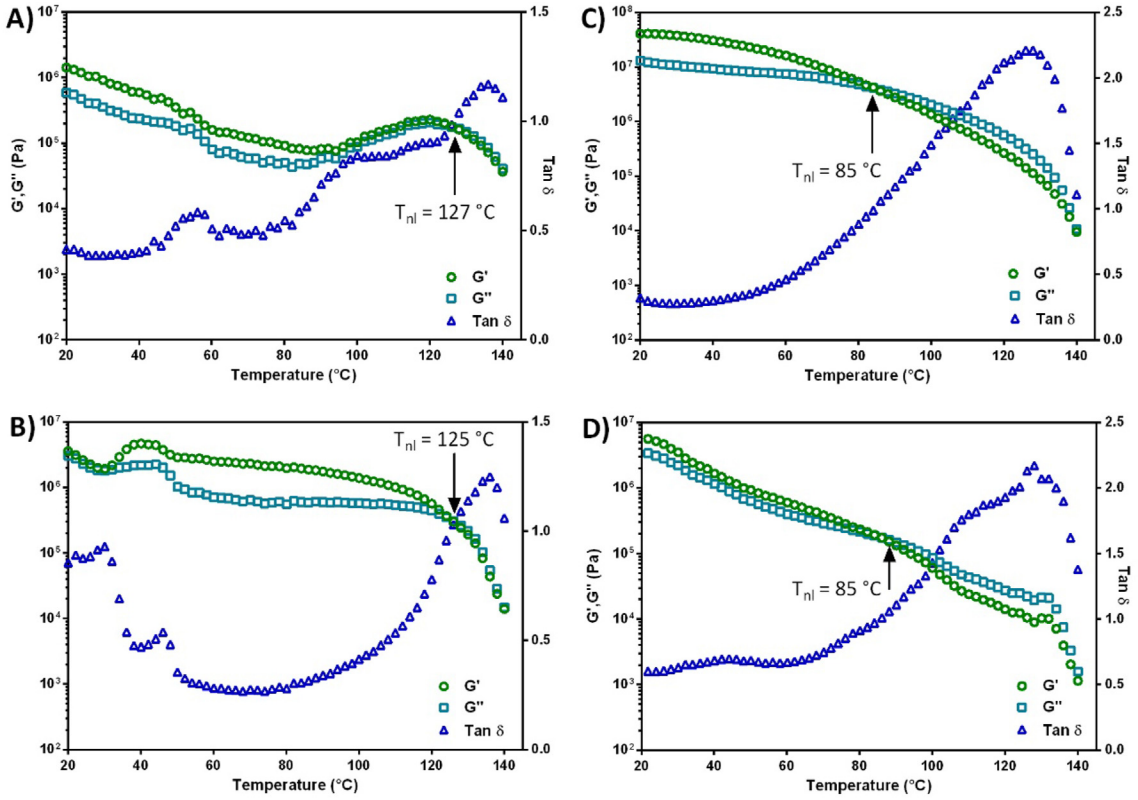

Fig. 5. G′, G″, and tan δ versus temperature for the supramolecular ionic networks $TA_1SA_0PA_0$ (A), $TA_{0.95}SA_{0.05}PA_0$ (B), $TA_{0.85}SA_{0.15}PA_0$ (C), and $TA_{0.75}SA_{0.25}PA_0$ (D).

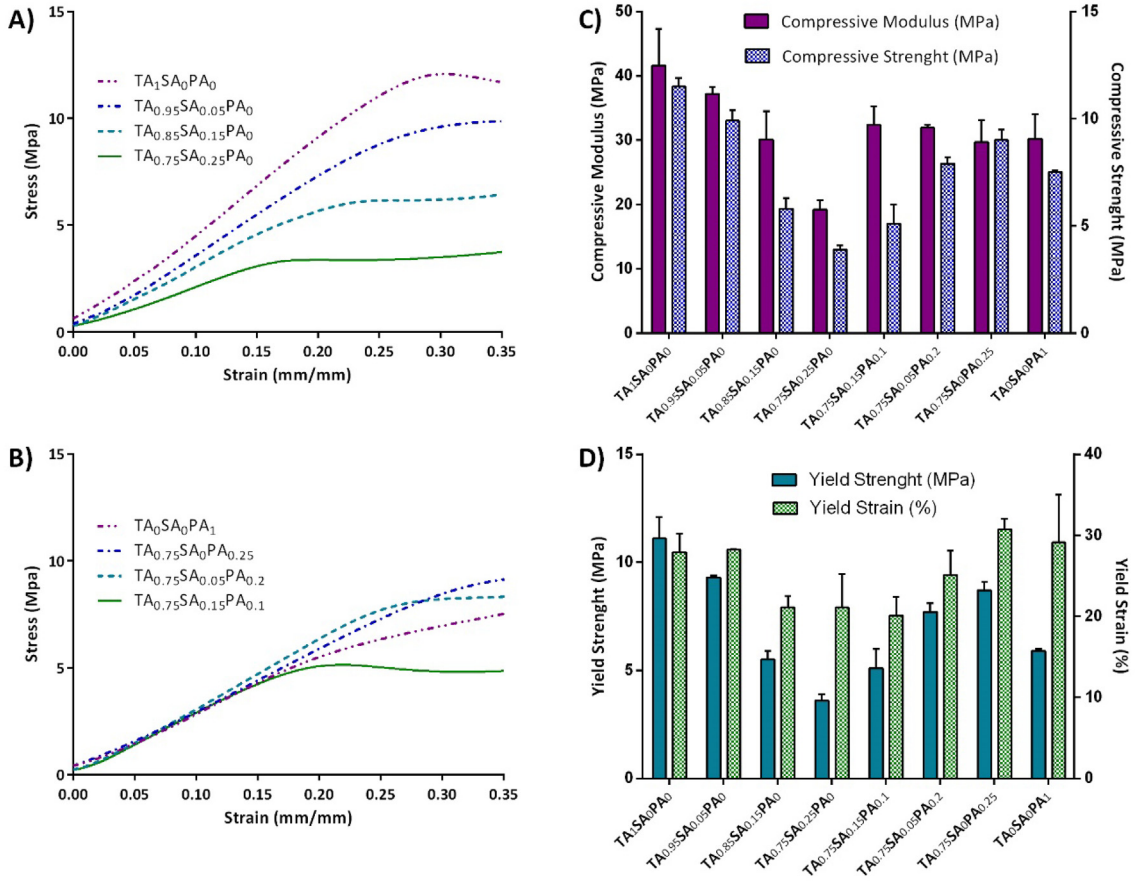

Fig. 6. Compressive stress versus strain curves (A, B), compressive modulus and compressive strength (C), yield strength, and yield strain (D) of the ionic networks.

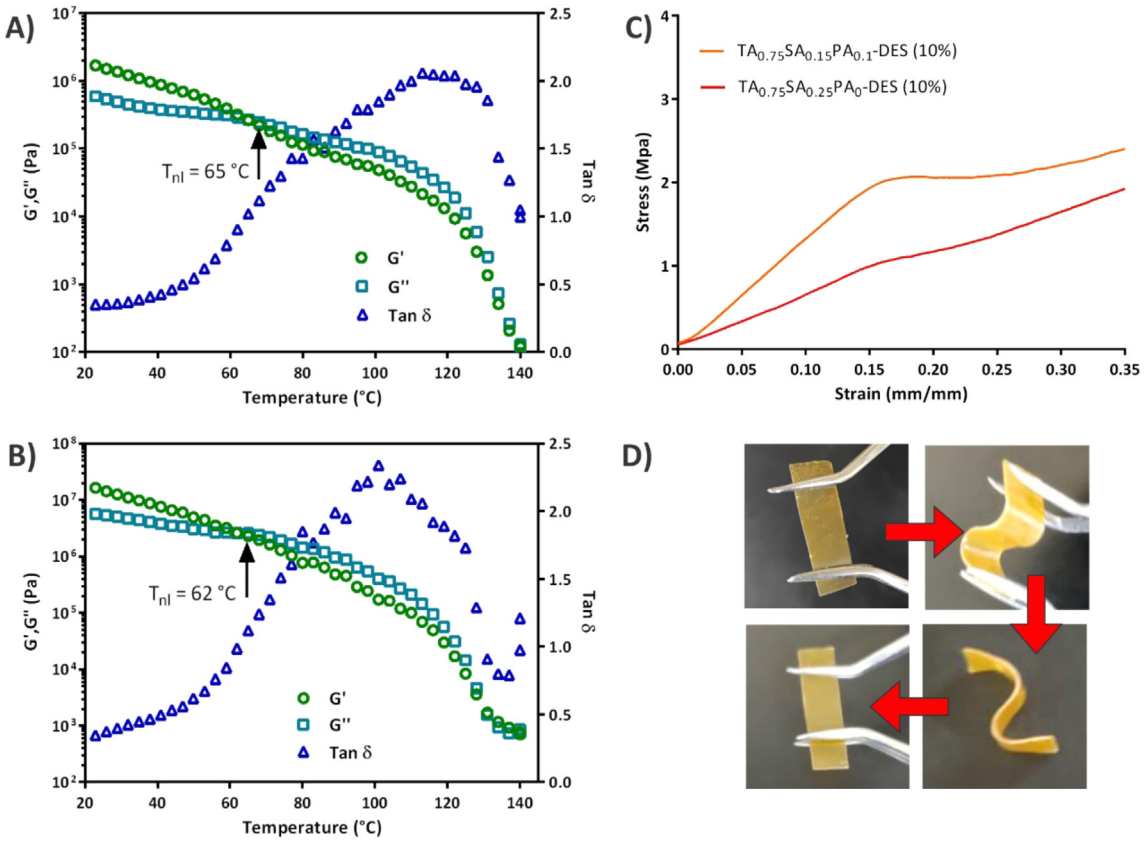

Fig. 7. G′, G″, and tan δ versus temperature for the supramolecular ionic networks $TA_{0.75}SA_{0.25}PA_0$-DES (10%) (A) and $TA_{0.75}SA_{0.15}PA_{0.1}$−DES (10%) (B). Compressive stress versus strain curves of DES-doped ionic networks (C). Photographs showing the flexibility of DES-doped ionic networks deformed into an "S" shape, the network permanence in the deformed shape, and its subsequent deformation to the original straight shape (D).

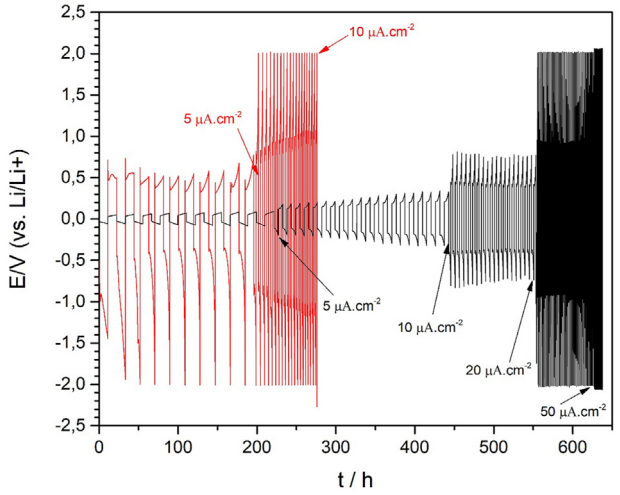

Fig. 8. Galvanostatic cycling of a symmetrical lithium cell assembled with $TA_{0.75}SA_{0.25}PA_0$ (red line) and $TA_{0.75}SA_{0.25}PA_0$-DES (10%) (black line) membranes at several current densities.

symmetric for lithium deposition-dissolution, and the cell reaches the potential limit quickly even for very low current density (5–10 μA/cm^2); therefore, this membrane was not suitable as a gel electrolyte for metallic lithium.

$TA_{0.75}SA_{0.25}PA_0$ and $TA_{0.75}SA_{0.25}PA_0$-DES (10%) membranes were also tested as gel polymer electrolytes in symmetric Li–Li cells. Both cells assembled with these membranes show typical potential profiles at different current densities (Fig. 8). The cell assembled with $TA_{0.75}SA_{0.25}PA_0$ in the first cathodic cycle at 5 μA/cm^2 shows the peak associated with the formation of nucleation seeds leading to lithium deposition [33–35]. For the next cycles, the potential shows the typical shape for a metal lithium cell with two peaks resulting from different kinetic pathways for reactions at the electrode/electrolyte interphase [35], reaching the potential limit during the cathodic scan. When the current increases to 10 μA/cm^2, the potential increases quickly for both anodic and cathodic cycles, reaching the potential limit after a few minutes, and the galvanostatic process is terminated by voltage limitation instead of time limitation. This increase in the voltage indicates a decrease in the ion concentration on the surface, that is, $TA_{0.75}SA_{0.25}PA_0$ cannot deliver Li^+ fast enough to enable the electrochemical reaction at that current density. Instead, the cell assembled with $TA_{0.75}SA_{0.25}PA_0$-DES (10%) could be cycled at 5, 10, and 20 μA/cm^2 without reaching the potential limit, and cycles are limited by potential just when the current increases to 50 μA/cm^2. These results show a clear improvement when an amount of DES is added to the membrane: $TA_{0.75}SA_{0.25}PA_0$-DES (10%) can deliver Li^+ to feed the electrochemical reaction for higher current densities than membrane $TA_{0.75}SA_{0.25}PA_0$. Even more, the $TA_{0.75}SA_{0.25}PA_0$-DES (10%) cells show, at 5 μA/cm^2, a square potential curve without peaking, which indicates a more stable interface with an easier stripping/deposition process.

The decomposition of the electrolyte at upper voltage affects both the safety and the performance of Li-metal batteries; therefore, it is necessary to have stable electrolytes at high potentials. The electrochemical windows of $TA_{0.75}SA_{0.25}PA_0$ and

$TA_{0.75}SA_{0.25}PA_0$-DES (10%) membranes were assessed by linear sweep voltage (Fig. S9). Both cells show an oxidation process up to 5.0 V and 4.5 V for membranes without and with DES, respectively. Even after the maximum peak, they can cycle to higher potentials without the occurrence of another oxidative process.

Although there is still plenty of room for improving the electrochemical performance of the eutectogels electrolytes, the insights gained with this proof of concept are quite encouraged, and future research efforts should be devoted to maximizing ionic conductivity and current density.

3. Conclusions

A set of fully biobased ionic networks were synthesized, combining SA, TA, PA, and Priamine™ 1071 at different mole ratios. It was demonstrated that incorporating SA ($TA_{0.75}SA_{0.25}PA_0$) and low PA contents decreases the T_m and crystallinity of the final ionic network, affording materials with excellent mechanical performance. All the ionic membranes were thermally stable until 170 °C in air and showed network-to-liquid transitions between 75 and 127 °C, finding a direct correlation between crystallinity and this phase transition. The ionic character of these supramolecular networks turns them into exciting platforms for hosting DES toward the rational design of dynamic eutectogels. As proof of this, the $TA_{0.75}SA_{0.25}PA_0$ network was miscible with a lithium-based eutectic mixture, opening the gate to explore its potential as a polymer gel electrolyte in symmetric Li—Li cells. The eutectogel membranes showed a promising working performance although with a limited current density.

Altogether, these results unveil the potential of the bioderived ionic networks as DES-supporting scaffolds, opening the doors to investigating an endless number of eutectic mixtures to develop innovative dynamic eutectogels.

Credit author statement

Ludmila I. Ronco: Conceptualization, Methodology, Validation, Formal analysis, Investigation, Writing – Original draft. **Gisela C. Luque:** Validation, Investigation, Writing – Original draft. **Cecilia A. Calderón:** Methodology, Validation, Investigation, Writing – Original draft. **Esteban M. Euti:** Methodology, Validation, Investigation. **Elena Rufeil Fiori:** Methodology, Validation, Investigation. **Daniel E. Barraco:** Resources. **Ezequiel P.M. Leiva:** Resources. **David Mecerreyes:** Writing – Review and editing. **Roque J. Minari:** Writing – Review and editing. **Matías L. Picchio:** Conceptualization, Resources, Writing – Review and editing, Supervision, Project administration, Funding acquisition.

Declaration of competing interest

The authors declare that they have no known competing financial interests or personal relationships that could have appeared to influence the work reported in this paper.

Data availability

Data will be made available on request.

Acknowledgments

Open Access funding provided by the University of Basque Country. The financial support received from CONICET and ANPCyT (PICT 2018-01032) (Argentina) is gratefully acknowledged.

Appendix A. Supplementary data

Supplementary data to this article can be found online at https://doi.org/10.1016/j.mtchem.2023.101525.

References

[1] L. Yu, F.B. Madsen, S. Hvilsted, A.L. Skov, Dielectric elastomers, with very high dielectric permittivity, based on silicone and ionic interpenetrating networks, RSC Adv. (2015), https://doi.org/10.1039/c5ra07375h.
[2] W. Yang, F. Liu, R. Li, X. Wang, W. Hao, Multiple stimuli-responsive fluorescent sensor from citric acid and 1-(2-aminoethyl)piperazine, ACS Appl. Mater. Interfaces (2018), https://doi.org/10.1021/acsami.7b17894.
[3] W. Mai, Q. Yu, C. Han, F. Kang, B. Li, Self-healing materials for energy-storage devices, Adv. Funct. Mater. (2020), https://doi.org/10.1002/adfm.201909912.
[4] M. Comí, G. Lligadas, J.C. Ronda, M. Galià, V. Cádiz, Adaptive bio-based polyurethane elastomers engineered by ionic hydrogen bonding interactions, Eur. Polym. J. (2017), https://doi.org/10.1016/j.eurpolymj.2017.04.026.
[5] A.V. Radchenko, H. Chabane, B. Demir, D.J. Searles, J. Duchet-Rumeau, J.F. Gérard, J. Baudoux, S. Livi, New epoxy thermosets derived from a bisimidazolium ionic liquid monomer: an experimental and modeling investigation, ACS Sustain. Chem. Eng. (2020), https://doi.org/10.1021/acssuschemeng.0c03832.
[6] A. Bossion, I. Olazabal, R.H. Aguirresarobe, S. Marina, J. Martín, L. Irusta, D. Taton, H. Sardon, Synthesis of self-healable waterborne isocyanate-free poly(hydroxyurethane)-based supramolecular networks by ionic interactions, Polym. Chem. (2019), https://doi.org/10.1039/c9py00439d.
[7] D. Wang, H. Zhang, B. Cheng, Z. Qian, W. Liu, N. Zhao, J. Xu, Dynamic crosslinks to facilitate recyclable polybutadiene elastomer with excellent toughness and stretchability, J. Polym. Sci. Part A Polym. Chem. (2016), https://doi.org/10.1002/pola.27983.
[8] M. Wathier, M.W. Grinstaff, Synthesis and properties of supramolecular ionic networks, J. Am. Chem. Soc (2008), https://doi.org/10.1021/ja803248q.
[9] M. Comí, M. Fernández, A. Santamaría, G. Lligadas, J.C. Ronda, M. Galià, V. Cádiz, Carboxylic acid ionic modification of castor-oil-based polyurethanes bearing amine groups: chemically tunable physical properties and recyclability, Macromol. Chem. Phys. (2017), https://doi.org/10.1002/macp.201700379.
[10] H. Daemi, S. Rajabi-Zeleti, H. Sardon, M. Barikani, A. Khademhosseini, H. Baharvand, A robust super-tough biodegradable elastomer engineered by supramolecular ionic interactions, Biomaterials (2016), https://doi.org/10.1016/j.biomaterials.2016.01.025.
[11] A. Noro, K. Ishihara, Y. Matsushita, Nanophase-separated supramolecular assemblies of two functionalized polymers via acid-base complexation, Macromolecules (2011), https://doi.org/10.1021/ma201440v.
[12] A. Bossion, R.H. Aguirresarobe, L. Irusta, D. Taton, H. Cramail, E. Grau, D. Mecerreyes, C. Su, G. Liu, A.J. Müller, H. Sardon, Unexpected synthesis of segmented poly(hydroxyurea-urethane)s from dicyclic carbonates and diamines by organocatalysis, Macromolecules (2018), https://doi.org/10.1021/acs.macromol.8b00731.
[13] M.A. Aboudzadeh, M.E. Muñoz, A. Santamaría, R. Marcilla, D. Mecerreyes, Facile synthesis of supramolecular ionic polymers that combine unique rheological, ionic conductivity, and self-healing properties, Macromol, Rapid Commun (2012), https://doi.org/10.1002/marc.201100728.
[14] M.A. Aboudzadeh, M.E. Muñoz, A. Santamaría, M.J. Fernández-Berridi, L. Irusta, D. Mecerreyes, Synthesis and rheological behavior of supramolecular ionic networks based on citric acid and aliphatic diamines, Macromolecules 45 (2012) 7599–7606, https://doi.org/10.1021/MA300966M/ASSET/IMAGES/LARGE/MA-2012-00966M_0010 (JPEG).
[15] M.A. Aboudzadeh, M.E. Muñoz, A. Santamaría, D. Mecerreyes, New supramolecular ionic networks based on citric acid and geminal dicationic ionic liquids, RSC Adv. (2013), https://doi.org/10.1039/c3ra40629f.
[16] M.A. Aboudzadeh, A.S. Shaplov, G. Hernandez, P.S. Vlasov, E.I. Lozinskaya, C. Pozo-Gonzalo, M. Forsyth, Y.S. Vygodskii, D. Mecerreyes, Supramolecular ionic networks with superior thermal and transport properties based on novel delocalized di-anionic compounds, J. Mater. Chem. (2015), https://doi.org/10.1039/c4ta05792a.
[17] A. Aboudzadeh, M. Fernandez, M.E. Muñoz, A. Santamaría, D. Mecerreyes, Ionic supramolecular networks fully based on chemicals coming from renewable sources, Macromol. Rapid Commun. (2014), https://doi.org/10.1002/marc.201300732.
[18] A.B. Burns, R.A. Register, Mechanical properties of star block polymer thermoplastic elastomers with glassy and crystalline end blocks, Macromolecules (2016), https://doi.org/10.1021/acs.macromol.6b02175.
[19] S. Liffland, M.A. Hillmyer, Enhanced mechanical properties of aliphatic polyester thermoplastic elastomers through star block architectures, Macromolecules (2021), https://doi.org/10.1021/acs.macromol.1c01357.
[20] J.-H. Kim, D.-H. Park, J.-S. Jang, J.-H. Shin, M.-C. Kim, S.-B. Kim, S.-H. Moon, S.-N. Lee, K.-W. Park, High-performance free-standing hybrid solid electrolyte membrane combined with Li6.28Al0.24La3Zr2O12 and hexagonal-BN for all-solid-state lithium-based batteries, Chem. Eng. J. 446 (2022), 137035, https://doi.org/10.1016/j.cej.2022.137035.

[21] M. Liu, X. Guan, H. Liu, X. Ma, Q. Wu, S. Ge, H. Zhang, J. Xu, Composite solid electrolytes containing single-ion lithium polymer grafted garnet for dendrite-free, long-life all-solid-state lithium metal batteries, Chem. Eng. J. 445 (2022), 136436, https://doi.org/10.1016/j.cej.2022.136436.
[22] M. Li, K. Wang, J. Liu, F. Shen, C. Xu, X. Han, Synergistically reinforced poly(-ethylene oxide)-based composite electrolyte for high-temperature lithium metal batteries, J. Colloid Interface Sci. 622 (2022) 1029–1036, https://doi.org/10.1016/j.jcis.2022.05.002.
[23] J.L. Olmedo-Martínez, L. Porcarelli, G. Guzmán-González, I. Calafel, M. Forsyth, D. Mecerreyes, A.J. Müller, Ternary poly(ethylene oxide)/Poly(l, l -lactide) PEO/PLA blends as high-temperature solid polymer electrolytes for lithium batteries, ACS Appl. Polym. Mater. 3 (2021) 6326–6337, https://doi.org/10.1021/acsapm.1c01093.
[24] S. Zhang, Y. Li, H. Zhang, G. Wang, H. Wei, X. Zhang, N. Ma, Bioinspired conductive hydrogel with ultrahigh toughness and stable antiswelling properties for articular cartilage replacement, ACS Mater. Lett. (2021), https://doi.org/10.1021/acsmaterialslett.1c00203.
[25] S. Zhang, Y. Zhang, B. Li, P. Zhang, L. Kan, G. Wang, H. Wei, X. Zhang, N. Ma, One-step preparation of a highly stretchable, conductive, and transparent poly(vinyl alcohol)-phytic acid hydrogel for casual writing circuits, ACS Appl. Mater. Interfaces (2019), https://doi.org/10.1021/acsami.9b12626.
[26] A. Boisset, S. Menne, J. Jacquemin, A. Balducci, M. Anouti, Deep eutectic solvents based on N-methylacetamide and a lithium salt as suitable electrolytes for lithium-ion batteries, Phys. Chem. Chem. Phys. 15 (2013) 20054–20063, https://doi.org/10.1039/c3cp53406e.
[27] W. Zaidi, A. Boisset, J. Jacquemin, L. Timperman, M. Anouti, Deep eutectic solvents based on N-methylacetamide and a lithium salt as electrolytes at elevated temperature for activated carbon-based supercapacitors, J. Phys. Chem. C 118 (2014) 4033–4042, https://doi.org/10.1021/jp412552v.
[28] T.T.A. Dinh, T.T.K. Huynh, L.T.M. Le, T.T.T. Truong, O.H. Nguyen, K.T.T. Tran, M.V. Tran, P.H. Tran, W. Kaveevivitchai, P.M.L. Le, Deep eutectic solvent based on lithium bis[(trifluoromethyl)sulfonyl] imide (LiTFSI) and 2,2,2-trifluoroacetamide (TFA) as a promising electrolyte for a high voltage lithium-ion battery with a LiMn2O4Cathode, ACS Omega 5 (2020) 23843–23853, https://doi.org/10.1021/acsomega.0c03099.
[29] B. Joos, T. Vranken, W. Marchal, M. Safari, M.K. Van Bael, A.T. Hardy, Eutectogels: a new class of solid composite electrolytes for Li/Li-ion batteries, Chem. Mater. (2018), https://doi.org/10.1021/acs.chemmater.7b03736.
[30] P. Dong, X. Zhang, K.S. Han, Y. Cha, M.K. Song, Deep eutectic solvent-based polymer electrolyte for solid-state lithium metal batteries, J. Energy Chem. 70 (2022) 363–372, https://doi.org/10.1016/j.jechem.2022.02.026.
[31] P. Jaumaux, Q. Liu, D. Zhou, X. Xu, T. Wang, Y. Wang, F. Kang, B. Li, G. Wang, Deep-eutectic-solvent-based self-healing polymer electrolyte for safe and long-life lithium-metal batteries, Angew. Chem., Int. Ed. 59 (2020) 9134–9142, https://doi.org/10.1002/anie.202001793.
[32] M.A. Aboudzadeh, M.E. Muñoz, A. Santamaría, R. Marcilla, D. Mecerreyes, Facile synthesis of supramolecular ionic polymers that combine unique rheological, ionic conductivity, and self-healing properties, macromol, Rapid Commun 33 (2012) 314–318, https://doi.org/10.1002/MARC.201100728.
[33] K.H. Chen, K.N. Wood, E. Kazyak, W.S. Lepage, A.L. Davis, A.J. Sanchez, N.P. Dasgupta, Dead lithium: mass transport effects on voltage, capacity, and failure of lithium metal anodes, J. Mater. Chem. A. 5 (2017) 11671–11681, https://doi.org/10.1039/C7TA00371D.
[34] C.A. Calderón, A. Vizintin, J. Bobnar, D.E. Barraco, E.P.M. Leiva, A. Visintin, S. Fantini, F. Fischer, R. Dominko, Lithium metal protection by a cross-linked polymer ionic liquid and its application in lithium battery, ACS Appl. Energy Mater. 3 (2020) 2020–2027, https://doi.org/10.1021/ACSAEM.9B02309/SUPPL_FILE/AE9B02309_SI_001.PDF.
[35] K.N. Wood, E. Kazyak, A.F. Chadwick, K.H. Chen, J.G. Zhang, K. Thornton, N.P. Dasgupta, Dendrites and pits: untangling the complex behavior of lithium metal anodes through operando video microscopy, ACS Cent. Sci. 2 (2016) 790–801, https://doi.org/10.1021/ACSCENTSCI.6B00260/SUPPL_FILE/OC6B00260_SI_001.MOV.